JOURNAL OF MATERIALS SCIENCE 8 (1973) 1717–1724

The sintering and morphology of interconnected porosity in UO_2 powder compacts

W. BEERÉ
Central Electricity Generating Board, Berkeley Nuclear Laboratories, Berkeley, Gloucestershire, UK

Uranium dioxide powder compacts of ~ 46% green density were sintered in flowing hydrogen at temperatures between 1500 and 1700° C. On annealing, the compacts readily formed an interconnected system of pores stabilized by grain boundaries. The volume of open porosity decreased with an activation energy of 4.6 J mol^{-1} at a rate controlled by grain growth. The grain-boundary migration removed the restraint on the porosity allowing shrinkage to commence. The compact surface area decreased with a higher activation energy of 6.0 J mol^{-1}. The mechanism proposed for the diminishing area was the smoothing of the faceted powder grains. Nucleation of atomic layers on the facets was shown to account for the high activation energy. The equilibrium shapes that may be adopted by interconnected porosity were calculated using a model in which simpler geometry was substituted for the real anticlastic surface curvature. The model demonstrated the stabilizing effect of increasing grain-boundary energy and the formation of closed pores.

1. Introduction

The sintering of UO_2 powder compacts may be usefully divided into three regimes comprising the formation of necks between particles, the diminution of interconnected porosity and the subsequent densification of isolated pores. The first regime has frequently been studied using dilatometry. Sintering occurs rapidly and may be measured at temperatures as low as 600° C [1, 2]. The final densification of isolated pores still situated on grain boundaries is much slower and necessitates temperatures above 1500° C to observe sintering [3].

The intermediate stage of sintering is characterized by interconnecting pores of complex geometrical shape. The sintering kinetics are further complicated by the green density of the original compact [4]. Compacts with green densities below ~ 50% sinter with a significant fraction of intragranular cavitation. Conversely, when the green density is greater than ~ 50%, the sintered microstructure consists entirely of intergranular cavitation at triple points.

The present paper investigates the sintering kinetics of UO_2 powder compacts of ~ 46% green density and demonstrates the relationship between grain growth and densification. The surface area of the interconnected pore system was measured by nitrogen adsorbtometry [5].

The morphology of the interconnected porosity was investigated by considering the energy of different possible configurations. Computer calculations of the configurational energy demonstrated the stable shapes. Reducing the cavity volume was shown to eventually result in the formation of a closed neck isolating the pore from the interconnecting system.

The morphology of porosity is important not only to an understanding of sintering but also in gas release from nuclear fuels. During gas release, inert gas accumulates on grain boundaries and along grain edges. The gas escapes to the surface by forming interconnected porosity. The formation of interconnected porosity is believed to be similar to the elimination of porosity during sintering.

2. Experimental

Cylindrical powder compacts 18 mm long and 8 mm diameter were made by compressing UO_2 powder to a load of 500 kg in a metal die lightly lubricated with a solution of stearic acid in ether. Sintering was carried out in a vertical alumina tube furnace at temperatures between 1500 and 1700°C in an atmosphere of flowing hydrogen. The furnace was continually run at temperature and specimens were inserted and withdrawn automatically to give a heating and cooling rate of $\sim$ 1°C sec^{-1}. Sintering was repeatedly interupted to measure the density and surface area of the compact.

Total porosity was calculated from the weight and from micrometer measurements of the compact size. The closed porosity was found by a hydrostatic comparitive technique [6]. The method consists of comparing the compact weight with that of a single crystal of UO_2 in air and after vacuum impregnation of methanol. Comparison with the fully dense material makes it unnecessary to know the densities of air and methanol. The absolute density of the UO_2 single crystal was checked to be certain that it contained no porosity.

The compact surface area was measured by nitrogen adsorption in a Perkin Elmer adsorbtometer by passing a mixture of nitrogen and helium over the compact at liquid nitrogen temperatures. The volume of adsorbed nitrogen was found for nitrogen partial pressures ranging between 0.08 and 0.63. The results were interpreted according to the BET Theory [7], by plotting P/V_a $(P_o - P)$ against P/P_o, Fig. 1, where P is the nitrogen partial pressure, P_o is atmospheric pressure, V_a is the absolute volume of adsorbed nitrogen and the surface area is proportional to the reciprocal of the slope. Since the plot passed through the origin of the graph it was possible to find the surface area from a single measurement and all subsequent readings were taken at a nitrogen partial pressure of 0.177.

TABLE I

Temperature (°C)	Time (min)	% cavitation			Surface area (m^2 g^{-1})
		Total	Closed	Open	
1500	20	30.5	0	30.5	0.720
	50	25.5	1.0	24.5	0.505
	125	20.4	1.4	19.0	0.318
	255	16.4	1.6	14.8	0.220
	515	13.7	2.7	11.0	0.124
	1000	12.0	3.2	8.8	0.083
	2000	10.6	4.0	6.6	0.041
	5900	8.2	4.5	3.7	—
1600	17	20.5	2.6	17.9	0.255
	152	14.1	3.8	10.3	0.084
	502	11.5	4.4	7.1	0.027
	1940	10.5	4.3	6.2	—
1700	17	12.7	4.2	8.6	0.080
	47	10.6	5.1	5.5	0.029
	111	9.8	5.3	4.5	—
	481	9.3	5.0	4.3	—

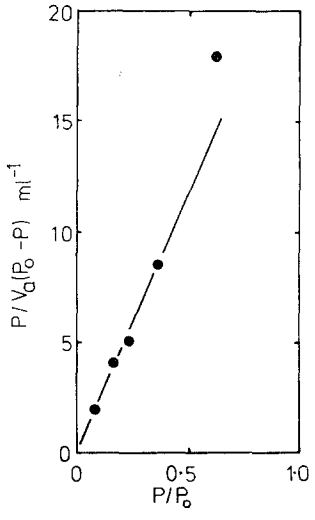

Figure 1 The BET [7] plot for the adsorption of nitrogen on a uranium dioxide powder compact.

3. Results and discussion

The surface area, open, closed and total porosity are given in Table I for three specimens annealed at 1500, 1600 and 1700°C. The amount of open porosity was calculated by subtracting the closed porosity from the total porosity. The porosity and surface area during sintering at 1500°C are shown in Fig. 2. The surface area diminished rapidly with sintering and accurate readings could not be taken below 0.04 m^2 g^{-1}.

The initial stage of sintering occurred very rapidly and was probably complete by the time the specimen had reached temperature. A further powder compact was annealed at 1450°C for 1 h and fractured. The scanning electron micrograph of the surface, Fig. 3a, shows the compact

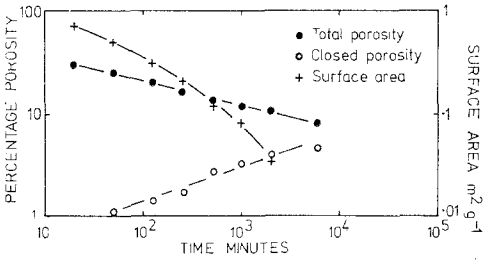

Figure 2 The porosity and surface area versus time for a compact annealed at 1500°C.

to consist of fine grains 0.2 to 0.3 μm across loosely bonded together.

Fig. 3b shows the fracture surface after 5900 min at 1500°C. The compact still contained regions of small faceted grains but with areas of higher density. Fig. 4a and b shows the nature of the fracture surface after 1940 min at 1600°C and 480 min at 1700°C, respectively. Although the compact densities were similar to that at 1500°C the structure appeared superficially denser with more rounded porosity.

The open porosity decreased with time as $\sim t^{-1/3}$ at 1500, 1600 and 1700°C. The results have been plotted against $t \exp(-Q/RT)$, Fig. 5, where Q is the activation energy, R the gas constant and T the absolute temperature. The points were closest to a single line for an activation energy of 4.6×10^5 J mol^{-1}.

The sintering results of low green density compacts are well interpreted by linking the removal of open porosity to grain growth. Kingery and Francois [8] have shown that the ability of pores to shrink or grow is related to the interfacial angles and number of grains surrounding a pore. The more grains surrounding a pore, the less likely it is to sinter and, hence, the lower the green density of a compact, the fewer the number of pores capable of sintering. The compact after the initial stage of sintering is envisaged as a system of stable interlinking pores held in place by the grain boundaries. During grain growth the boundaries migrate off the pores, freeing the surfaces from restraint. The cavitation may now decrease in volume and form a neck which closes, producing an intragranular pore. The fraction of open cavitation, $\Delta\rho/\rho$, at any stage of grain growth depends, to a first approximation, on the amount of grain boundary still binding porosity. If D is the instantaneous grain size then the surface area of grains/unit volume is proportional to $1/D$. It is assumed

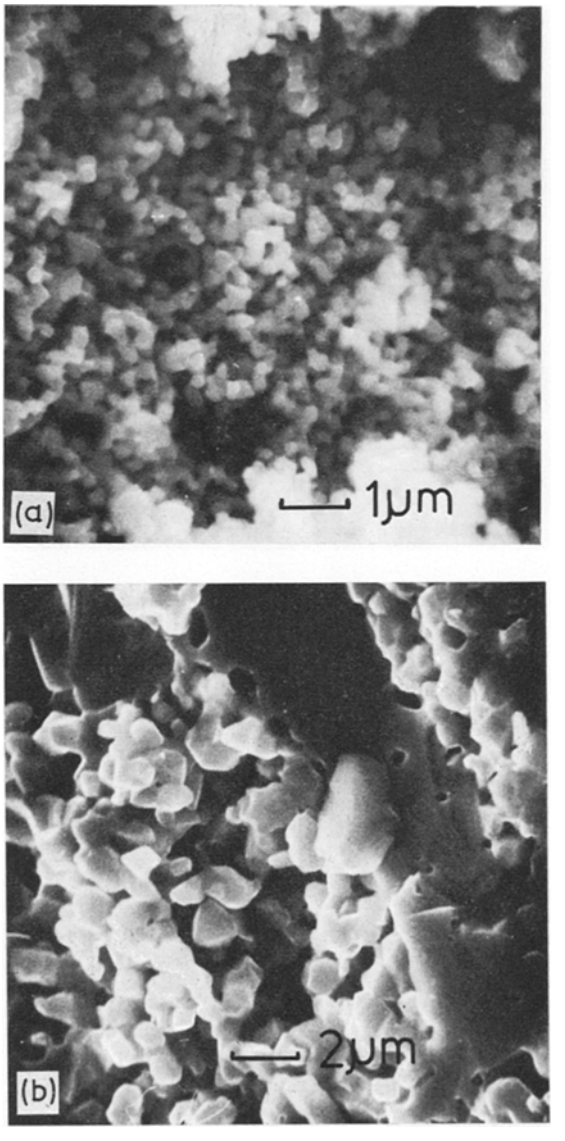

Figure 3 (a) A scanning electron microscope fractograph of a UO_2 powder compact annealed at 1450°C for 1 h. (b) Annealed for 5900 min at 1500°C.

the bound porosity changes little in volume before boundary migration, then the fraction of open porosity is proportional to $1/D$. If $(\Delta\rho/\rho)_0$ is the fractional cavitation level after the initial neck growth stage and D_0 the corresponding grain size, then

$$\left(\frac{\Delta\rho}{\rho}\right) = \left(\frac{\Delta\rho}{\rho}\right)_0 \frac{D_0}{D} \cdot \qquad (1)$$

After 5900 min at 1500°C, the fraction of

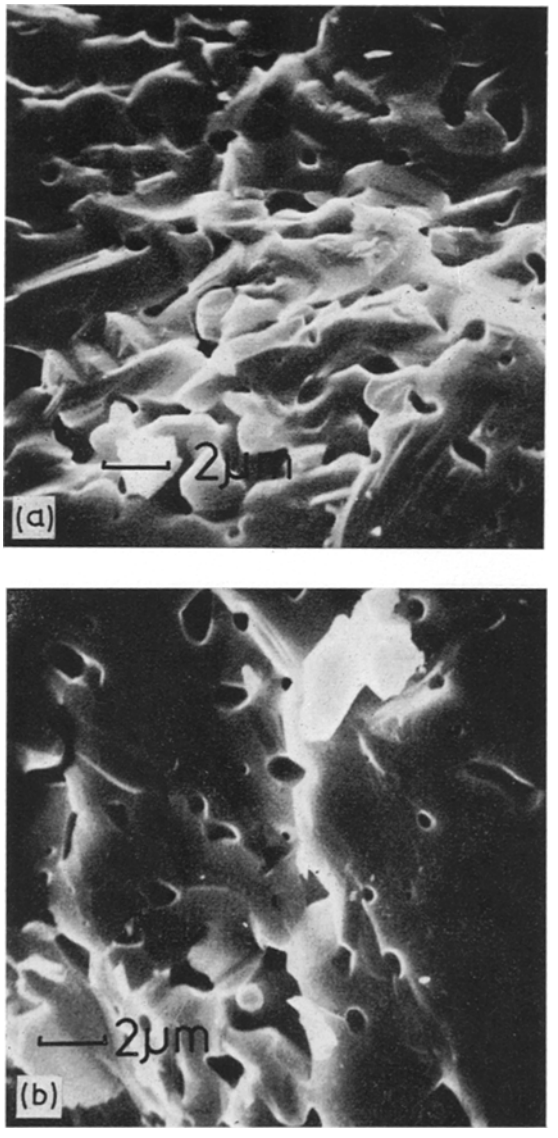

Figure 4 (a) A scanning electron microscope fractograph of a UO_2 powder compact annealed for 1940 min at 1600°C. (b) Annealed for 481 min at 1700°C.

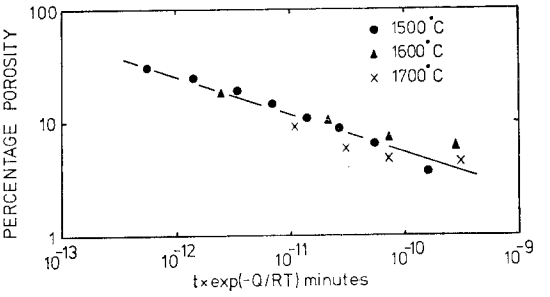

Figure 5 The percentage open porosity versus diffusion rate compensated time for specimens annealed at 1500, 1600 and 1700°C.

open porosity was $\sim 4\%$ and the mean linear intercept grain size was ~ 4 μm.

The initial fraction of porosity was $\sim 50\%$, then from Equation 1 D_0 was 0.3 μm. Reference to Fig. 3a shows 0.3 μm to be in good agreement with the initial crystallite size. Grain growth rates in porous compacts have been shown to follow the form

$$D^n = D_0^n + \alpha\, t \exp(-Q/RT) \qquad (2)$$

where α and n are constants. The value of n has been reported as 2.5 in UO_2 of $\sim 97\%$ dense [9], with an activation energy of 4.6×10^5 J mol^{-1}. Mansour and White [10], annealed pellets of $\sim 50\%$ green density at 1400°C and found n took on a value of 3.

Taking the value of 3 for n, then when $D_0 \ll D$, from Equations 1 and 2

$$\left(\frac{\Delta\rho}{\rho}\right)^{-3} = \text{const. } t \exp(-Q/RT). \qquad (3)$$

Equation 3 is in excellent agreement with the results in Fig. 5.

The rate of decrease in surface area, dS/dt, was compared with the rate of decrease in open porosity $d/dt\ (\Delta\rho/\rho)$. When the dimensions of surface area were taken to be m^2/m^3, the ratio $d(\Delta\rho/\rho)/dS$ was found to be ~ 0.03 μm at 25% open porosity increasing to ~ 0.06 μm at 7% open porosity. The ratio $d(\Delta\rho/\rho)/dS$ takes on a value $-r/2$, for a porous composite consisting of spherical cavities of radius r, shrinking by bulk diffusion. The corresponding value for cylinders of radius r is $-r$. The values for spheres and cylinders separating from the open porosity by the formation of closed necks is $-r/3$ and $-r/2$ for spheres and cylinders respectively. The observed value of 0.03 μm is smaller than would be expected for the cavity sizes observed in the fractographs, Figs 3 and 4.

The small observed value may be accounted for if the faceted surface smooths and the surface area diminishes without a reduction in the volume of open porosity. The activation energy for the rate of decrease of surface area was significantly higher than that for grain growth. Fig. 6 shows the surface area plotted versus $(t \exp(-Q/RT))/T$, where t is time. A best fit was obtained when $Q \sim 6 \times 10^5$ J mol^{-1}, a value close to the activation energy for evapora-

tion but higher than those normally observed for volume, surface and grain-boundary diffusion in UO_2. Reference to diffusion rates in bubbles of the same size as the porosity [11], shows that an evaporation-condensation mechanism is unlikely to produce surface smoothing in compacts at the temperatures in question.

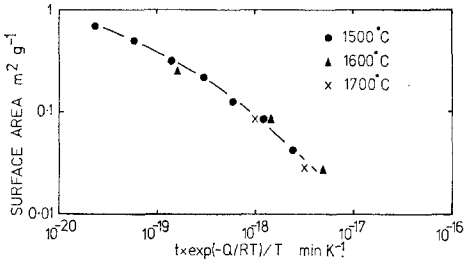

Figure 6 The surface area versus diffusion rate compensated time.

The high activation energy observed for the reduction in surface area may result from the effect of the faceted surface on the surface diffusion. Surface diffusion on faceted bubbles has been shown to result in significant material transport at 1400 to 1700°C but with a higher apparent activation energy than diffusion on smoothly rounded internal surfaces. Following a similar argument used for faceted bubbles [12], the apparent activation energy may be calculated in the following manner.

The free energy ΔG, required to form on an atomically smooth facet, a circular nucleus of radius r one atom layer thick is given by

$$\Delta G = 2\pi r\epsilon + \pi r^2 \lambda \, \Delta G_V \qquad (4)$$

where ϵ is the step energy per unit length, λ the distance between atomic layers and ΔG_V the change in energy on moving unit volume of atoms to the nucleus. Differentiating Equation 4 and putting $\mathrm{d}\,\Delta G/\mathrm{d}r = 0$, the size of a critical nucleus r^* is given by

$$r^* = -\epsilon/\lambda \, \Delta G_V \qquad (5)$$

and the critical nucleation energy is

$$\Delta G^* = \pi \epsilon r^*. \qquad (6)$$

If R is the radius of the crystallites forming the facets, Fig. 3a, and γ the energy of the surface, then

$$\Delta G_V = -2\gamma/R. \qquad (7)$$

From Equations 5 to 7

$$\Delta G^* = \pi \epsilon^2 R/2\lambda\gamma. \qquad (8)$$

Taking $\epsilon = 7 \times 10^{-12}$ J m^{-1} [12], $\lambda = 0.5 \times 10^{-9}$ m, $\gamma = 0.2$ J m^{-2} [13] and putting $R = 0.3$ μm, then from Equation 8 $\Delta G^* = 1.5 \times 10^5$ J mol^{-1}.

The nucleation rate of atomic layers and, hence, the atom flux is proportional to the product of the rate of jumping of surface atoms onto the nucleus and the probability that the nucleus grows to a critical size. Since the first term of the product is proportional to the surface diffusion coefficient and the second is proportional to the exponential of the critical nucleation energy, the apparent activation energy is the sum of those for the two processes. Taking a value of 4.5×10^5 J mol^{-1} for the surface diffusion activation energy [14] the apparent activation energy is 6×10^5 J mol^{-1} in good accord with the experimental value.

3.1. The equilibrium shapes of interconnecting porosity

The equilibrium shape adopted by porosity occurs when the change in free energy with change in shape and volume is zero. If E is the free energy of the pore of volume V and surface area A_S, and A_g is the surface area of grain boundary occupied by the pore, then

$$E = \gamma_S A_S - \gamma_g A_g \qquad (9)$$

where γ_S and γ_g are the surface and grain-boundary energies respectively. Equilibrium exists when the partial differential coefficients are zero, i.e. $\partial E/\partial V = \partial E/\partial A_S = 0$.

The equilibrium shape of porosity not stabilized by gas is often that with zero volume. In order to calculate the shape of porosity shrinking slowly, but with rapid surface diffusion maintaining all points on the surface at a constant potential, it is necessary to impose a limitation on the pore volume. The equilibrium shape adopted is that for which the change in free energy is zero during a small change in shape at constant volume. The configuration of minimum energy subject to a constant volume may be calculated by finding the minimum of the function Φ given by the equation

$$\mathrm{d}\Phi = \mathrm{d}E - \eta \mathrm{d}V \qquad (10)$$

where η is a Lagrangian multiplier.

From Equations 9 and 10 and differentiating

$$\mathrm{d}\Phi = \gamma_S \, \mathrm{d}A_S - \gamma_g \mathrm{d}A_g - \eta \, \mathrm{d}V. \qquad (11)$$

The equilibrium shape of gas filled pores may be found by incorporating into Equation 9 the work done on the enclosed gas. The change in energy upon a small change in shape and volume is

$$\mathrm{d}E = \gamma_S \, \mathrm{d}A_S - \gamma_g \, \mathrm{d}A_g - p\mathrm{d}V \qquad (12)$$

where p is the gas pressure. Equations 11 and 12 are identical with identical solutions. Voids shrinking slowly have the same shape and interfacial angles as stabilized gas bubbles of the same volume. A detailed analysis of lenticular bubbles [15] obtained the same result.

The exact equilibrium shapes of interconnected porosity are difficult to calculate because the surfaces have complex anticlastic curvature. Approximate solutions may be found by substituting shapes with simpler geometry. Fig. 7a shows a pore system intersected by three grain boundaries, interconnecting round a tetrakaidecahedron grain [16]. The volume and surface area of the porosity and the grain-boundary area removed by the porosity are given in the Appendix. The octahedron and triangular frustums, Fig. 7b, are more appropriate as the ratio of grain-boundary energy to surface energy γ_g/γ_s, tends to 1.7 whilst the sphere and conical frustums, Fig. 7c, are a better approximation as γ_g/γ_s tends to zero.

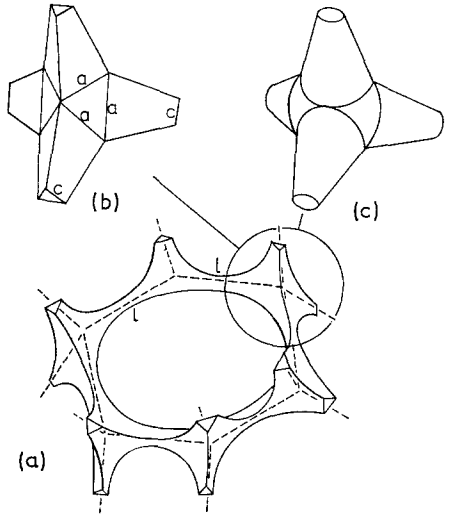

Figure 7 (a) The system of porosity interconnecting round a tetrakaidecahedron grain of length of side l. (b) An octahedron and four triangular frustrums where a is the length of side of the octahedron and c is the length of side at the neck. (c) A sphere and four conical frustrums where $a/\sqrt{3}$ is the radius of the sphere and $c/\sqrt{3}$ is the radius at the neck.

The free energy of the configuration of Fig. 7c was computed by allowing a/l_0 and c/l_0 to vary whilst keeping the pore volume constant, where $a/\sqrt{3}$ is the radius of the sphere at the grain corner, $c/\sqrt{3}$ is the radius in the neck region and l_0 is the initial length of side of the tetrakaidekahedron grain. Fig. 8 shows the dimensionless free energy versus c/l_0 for $\gamma_g = 0$, corresponding to the case when the grain boundaries have migrated from the porosity. Minima occur in the free energies for porosities between 30 and 14% indicating the existence of equilibrium shapes. Between 14 and 8% the energy curves are flat within the accuracy of the model but below 8% the free energy decreases with a decrease in neck size indicating that no stable interconnected pores exist. The relationship between fractional porosity volume and neck size for equilibrium configurations was computed for different values of γ_g/γ_s. The results are plotted in Fig. 9. The greater the grain-boundary energy, the smaller the minimum stable pore volume before the interconnected necks close. Grain boundaries have the effect of stabilizing interconnecting porosity. When grain boundaries migrate, the neck will close when the local cavitation level has fallen below 10 to 12%. Increasing the number of grain boundaries intersecting the porosity will increase the neck stability.

As the number of grain boundaries intersecting a pore are increased, in order to maintain a constant interfacial angle at the surface grain-boundary intersection, the surface curvature reduces and eventually changes sign. For

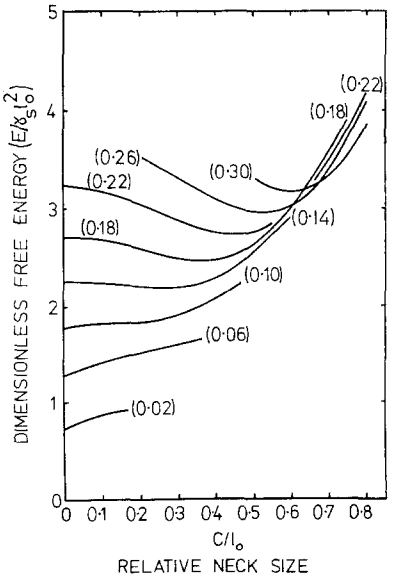

Figure 8 The free energy of the pore system versus the size of the connecting neck when the grain-boundary energy is zero.

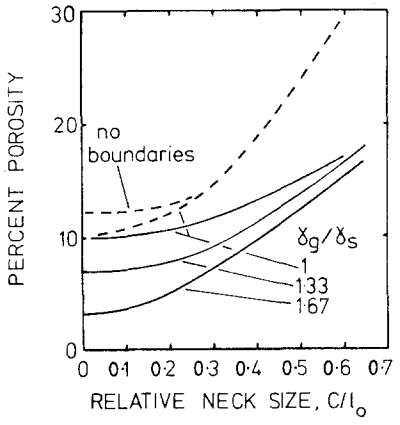

Figure 9 The fractional pore volume of interconnected equilibrium configurations versus neck size. The dotted and continuous lines correspond to energy curves for the sphere and conical frustrums Fig. 7c and for the octahedron and triangular frustrums Fig. 7b, respectively.

instance if the interfacial angle is $\pi/2$ radians and four boundaries intersect a cylinder, the cylinder becomes a square prism. Decreasing the number of boundaries makes the surfaces concave and increasing the number makes the surfaces convex. The vacancy concentration on a convex surface is less than the concentration on a plane surface and the porosity tends to grow rather than form closed necks.

4. Conclusions

Uranium dioxide powder compacts of 46% green density were annealed at temperatures between 1500 and 1700°C. The interconnected porosity resulting from the initial bonding of particles, sintered producing intragranular porosity. The decrease in volume of interconnected porosity was controlled by the increase in grain size. Grain boundaries migrating from pores released the surfaces allowing shrinkage and the subsequent formation of closed necks. The activation energy for sintering was 4.6×10^5 J mol^{-1}.

The surface area decreased rapidly with an activation energy of 6.0×10^5 J mol^{-1}. The large activation energy was interpreted as resulting from the smoothing of the faceted surface. The increase in apparent activation energy over that for surface diffusion was shown to be consistent with a nucleation mechanism on micron-sized crystals.

The equilibrium shapes of interconnected porosity were calculated from a simplified model, which considered porosity intersected by three grain boundaries. The porosity was stable down to local cavitation levels of about 10%. Increasing the grain-boundary energy increased the stability and decreased the volume at which the necks collapsed resulting in isolated pores.

Appendix

The volume V, the surface area A_s and the grain-boundary area A_g removed by the octahedron and triangular frustums of Fig. 7b are

$$V = 0.471\,a^2 + \frac{1}{\sqrt{3}}\left(\frac{l}{2} - \frac{a}{\sqrt{6}}\right)(a^2 + ac + c^2)$$

$$A_s = \sqrt{3}\,a^2 + 6(a + c)\sqrt{\left[\left(\frac{l}{2} - \frac{a}{\sqrt{6}}\right)^2 \times \frac{(a-c)^2}{12}\right]}$$

$$A_g = 6\left[\left(\frac{l}{2} - \frac{a}{\sqrt{6}}\right)\left(\frac{a+c}{\sqrt{3}}\right) \times \frac{a^2}{\sqrt{18}}\right]$$

where a is the length of side of the octahedron, c is the length of side at the neck and l is the length of side of the tetrakaidecahedron.

The corresponding equation for the sphere and concial frustums of Fig. 7c are

$$V = \frac{\sqrt{2}\pi}{3}a^3 + \frac{4\pi}{9}\left(\frac{l}{2} - \frac{a}{\sqrt{6}}\right)a^2 + ac + c^2 - \frac{4\pi}{3}a^3\left(\frac{l}{\sqrt{2}} - \frac{a}{\sqrt{6}}\right)^2\left(\sqrt{2} + \frac{l}{\sqrt{6}}\right)$$

$$A_s = 4\pi\left\{\left(\frac{a+c}{\sqrt{3}}\right)\sqrt{\left[\left(\frac{l}{2} - \frac{a}{\sqrt{6}}\right)^2 + \frac{(a-c)^2}{3}\right]} - \frac{a^2}{2} + \frac{a^2}{\sqrt{3}}\right\}$$

$$A_g = 6\left[\left(\frac{1}{2} - \frac{a}{\sqrt{6}}\right)\frac{(a+c)}{\sqrt{3}} + \frac{a^2}{\sqrt{18}}\right]$$

where $a/\sqrt{3}$ is the radius of the sphere and $c/\sqrt{3}$ is the radius at the neck.

Acknowledgement

This paper is published by permission of the Central Electricity Generating Board.

References

1. R. V. LENEL, *Phys. Sintering* 4 (1972) 1.
2. J. L. WOODFREY, *J. Amer. Ceram. Soc.* **55** (1972) 383.
3. B. BURTON and G. L. REYNOLDS, *J. Nucl. Mater.* **45** (1972) 10.
4. B. FRANCOIS and W. D. KINGERY, in "Sintering and Related Phenomena", (edited by G. C. Kucynski, N. A. Hooton and C. F. Gibbon) (Gordon and Breach, New York, 1967) p. 499.
5. C. A. ELYARD, *Powder Met* **12** (1963) 44.

6. R. T. RATCLIFFE, *Brit. J. Appl. Phys.* **16** (1965) 1193.
7. S. BRUNAUER, P. H. EMMETT and E. TELLER, *J. Amer. Chem. Soc.* **60** (1938) 309.
8. W. D. KINGERY and B. FRANCOIS, in "Sintering and Related Phenomena" (edited by G. C. Kuczynski *et al*) (Gordon and Breach, New York, 1967) p. 471.
9. J. R. MACEWAN and J. HAYASHI, *Proc. Brit. Ceram. Soc.* **7** (1965) 245.
10. N. A. L. MANSOUR and J. WHITE, *Powder Met.* **12** (1963) 108.
11. R. W. WEEKS, R. O. SCATTERGOOD and S. R. PATI, *J. Nuclear Mat.* **35** (1970) 223.
12. W. BEERÉ, *ibid*, **45** (1972) 91.
13. E. N. HODKIN and M. G. NICHOLAS, AERE Report No. AERE-R7066 (1972).
14. P. S. MAYA, *J. Nuclear Mat.* **40** (1971) 57.
15. G. L. REYNOLDS, W. BEERÉ and P. T. SAWBRIDGE, *ibid* **41** (1971) 112.
16. W. BEERÉ and G. L. REYNOLDS, *ibid*, **47** (1973) 51.

Received 29 May and accepted 27 June 1973.